Polymer Chemistry

Accepted Manuscript

ROYAL SOCIETY OF CHEMISTRY

www.rsc.org/polymers

Influence of Secondary Structure on the AIE-Related Emission Behavior of Amphiphilic Polypeptide Containing a Hydrophobic Fluorescent Terminal and Hydrophilic Pendant Groups

Li-Yang Lin, Po-Chiao Huang, Deng-Jie Yang, Jhen-Yan Gao and Jin-Long Hong*

Department of Materials and Optoelectronic Science, National Sun Yat-Sen University, Kaohsiung 80424, Taiwan

Study on an amphiphilic polypeptide of TP-PPLG-*g*-MEO_2 containing a hydrophobic tetraphenylthiophene (TP) terminal, with aggregation-induced emission (AIE) properties, and hydrophilic ether side groups evaluated that secondary structures (α-helix, β-sheet and random coil) of the peptide chains affected the AIE-related emission of the TP terminal. The amphiphilic TP-PPLG-*g*-MEO_2, prepared from ring-opening polymerization and the following click reaction, contained a secondary structure with the majority of α-helical chain. The main α-helical chain nevertheless can be converted into β-sheet structure by adding NaCl into the aqueous solution of TP-PPLG-*g*-MEO_2 and by that, the solution emission can be enhanced. In addition, the coil chain generated in the alkaline solution was found to emit efficiently with the highest emission intensity among all three conformations. Relationship between AIE property and secondary structure of peptide chains can be therefore evaluated. All three secondary structures were also used as luminescent sensors to test their sensitivity for bovine serum albumin (BSA).

INTRODUCTION

Since the first-discovered silole-derivative of 2,3,4,5,6-pentaphenyl-1-methylsilole[1,2] (PMS) as luminogen with aggregation-induced emission (AIE) properties, many AIE-active luminogens (AIEgens)[3-1] have been prepared and characterized regarding their unique feature that the dilute, non- or weakly-emissive solution of AIEgen can be tuned to emit intensely in the solution aggregated and solid states. Theoretical study suggested that restricted intramolecular rotation (RIM) of non-planar, propeller-shape AIEgens[10-12] in the solution aggregated and solid states is the inherent mechanism responsible for the enhanced emission of AIEgens. With regard to the promising emission properties, several AIEgens had been explored in the high-tech applications such as optoelectronic materials,[13-16] chemical sensors[17-19] and biomedical probes[20,21].

Synthetic polypeptides have been under considerable investigations regarding their potential applications in various scientific fields and close relationship to proteins[22-32]. The secondary structures (α-helix, β-sheet and random coil) of peptide chains are cornerstones for the construction of the well-defined tertiary structure of proteins, therefore, study on the synthetic polypeptide and its chain conformations in organic solvents illustrated one of the major efforts dedicated previously for understanding the complicated protein-protein interactions. In this respect, several traditional luminogens (such as carbazolyl,[33] dansyl[34] and pyrene[35]) had been chemically incorporated with synthetic polypeptides in order to monitor chain conformation of the polypeptides in solutions. For example, no excimer emission was detected for the pyrene-labeled polypeptide[35] since pyrene groups were well separated from each other by the polypeptide chains.

AIEgens were previously incorporated with synthetic polypetides[36,37] with the purpose to detect conformational change of the peptide chain by AIE-related emission. An AIEgen of tetraphenylthiophene (TP) was served as terminal and central units of poly(benzyl-L-glutamate)s (PBLGs) in the synthetic polypeptides of TP1PBLG and TP2PBLG,[36] respectively. Because that intermolecular aggregation of TP centers in TP2PBLG is sterically blocked by the large α-helical chains of TP2PBLG, solution of TP2PBLG is lower in emission than solution of TP1PBLG, whose TP terminal can be readily approached by other TP terminals to result in aggregates with high emission intensity. Adding trifluoroacetic acid (TFA) to solution of TP2PBLG converted the rigid α-helical chain into flexible random coil; after that, the emission intensity of TP2PBLG was largely raised due to the easy aggregation of the TP centers in the flexible coil chains. In contrast to the hydrophobic TP1PBLG and TP2PBLG, a water-soluble, TP-terminated polypeptide containing ionic sulfonate pendent groups[37] was synthesized later and characterized to exhibit a pH-induced helix-to-coil transition in the alkaline aqueous solution. Again, emission of this ionic polypeptide in alkaline solution was enhanced to a great extent due to the easy aggregation of the TP terminals in the coil chains.

The above examples[36,37] suggested the crucial roles of random coil and α-helix structures in enhancing and weakening the AIE-related emission, respectively, of the synthetic polypeptides. Despite the early efforts, correlation between β-sheet structure and AIE activity is still in demand due to the lack of reliable way in generating peptide chain containing the majority of β-sheet structure. This question can nevertheless be solved recently since we found that the fraction of β-sheet conformation can be largely enhanced by adding NaCl salt into the aqueous solution of an amphiphilic polypeptide of TP-PPLG-*g*-MEO_2 (Scheme 1). With a hydrophobic

TP terminal and hydrophilic methyl bis(ethylene oxide) (MEO_2) etheric side groups, the target polypeptide of TP-PPLG-*g*-MEO_2 is amphiphilic and can be prepared from a two-step reaction procedure including ring-opening polymerization (ROP) of PLG-NCA monomer initiated by an amino-functionalized AIEgen of TP-NH_2 and the following click reaction for the introduction of the MEO_2 side groups. The amphiphilic TP-PPLG-*g*-MEO_2, containing the majority of α-helical chains, can be dispersed in the salt and in the alkaline aqueous solutions to generate the respective β-sheet and random-coil chains for correlating their AIE-related emission behavior with the secondary structures of the peptide chains. This correlation is meaningful in considering that aggregation tendency and the corresponding AIE-related emission of the TP terminal in TP-PPLG-*g*-MEO_2 is essentially controlled by conformation of peptide chain connecting to TP terminal; that is, aggregation of the TP terminals is affected by the neighboring peptide chains of different chain conformations and so is the aggregation-related AIE emissive behavior. Besides theoretical correlation between conformational change and AIE activity, all three secondary structures generated in this study were further employed as luminescent sensors for the natural protein of bovine serum albumin (BSA). Corresponding luminescence responses can be used to evaluate how well the individual secondary structure complexed to BSA. The complexation tendency is strongly related to the aggregated level of the TP terminals in the large peptide matrix of BSA.

■ EXPERIMENTAL SECTION

Materials. DMF (Aldrich) was refluxed and distilled over CaH_2 (Aldrich) under nitrogen atmosphere to a flask containing alumina before use. CuBr (98%, Aldrich) was stirred overnight in acetic acid, filtered, washed with ethanol and diethyl ether,

and then dried in vacuum before use. Compounds of TP-NH_2[38], MEO_2-N_3[39] and γ-propargyl-L-glutamate N-carboxyanhydride (PLG-NCA)[40,41] were prepared according to the reported procedures. Polypeptides of TP-PPLG and TP-PPLG-*g*-MEO_2 were synthesized from the procedures given below:

Ring-opening polymerization of N-carboxyanhydride PLG-NCA to prepare TP-PPLG. Solution of PLG-NCA (3 g, 14.2 mmol) in anhydrous DMF (20 mL) was stirred and bubbled with argon for 20 min before adding solution of $TPNH_2$ (0.03 mL, 0.48 mmol) in anhydrous DMF (5 mL). The reaction mixture was stirred for 2 days at room temperature and the resulting polymer was precipitated from diethyl ether, and dried in vacuum oven. ^{1}H NMR (500 MHz, CD_2Cl_2): δ 8.34 (broad, H_f), 7.5-7.03 (broad, 19H, H_g), 4.68 (s, H_b), 3.98 (broad, H_e), 2.72 (broad, 2H, H_c), 2.48 (s, 1H, H_a), 2.32-2.19 (broad, 2H, H_d) (Figure 2a). ^{13}CNMR (125 MHz, CD_2Cl_2): δ 177.2, 173.0, 132-128, 79.3, 76.0, 57.5, 52.9, 31.9, 26.4. (Figure S5a).

Preparations of TP-PPLG-*g*-MEO_2 by click reaction. MEO_2-N_3 (0.15g, 0.8 mmol), TP-PPLG (0.1g, 0.6 mmol), and CuBr (0.03g, 0.12 mmol) were dissolved in DMF (25 mL) in a two-neck flask equipped with a magnetic stirrer and a condenser. After three freeze-thaw-pump cycles, ligand N,N,N',N",N"-pentamethyldiethylenetriamine (0.02ml, 0.12mmol) was added. Whole reaction mixtures were further subjected to three freeze-thaw-pump cycles before heated at 60 ^{o}C for 24 h. After cooling to room temperature, the resulting mixtures were passed through a neutral alumina column to remove the copper catalysts. The solution was then concentrated by rotary evaporation and precipitated from diethyl ether. The precipitate was filtered off and dried under vacuum at room temperature to obtain the final yellow-white product. TP-PPLG-*g*-MEO_2: ^{1}H NMR (500 MHz, d_6-DMSO/DCl(tiny)) 34 (s, $H_{f'}$), 8.14 (s, $H_{h'}$), 7.22-7.03 (broad, 19H, $H_{g'}$), 5.23-5.11 (s, $H_{b'}$), 4.50 (t, $H_{i'}$), 3.83 (t, $H_{j'}$), 3.54 (t,

$H_{k'}$), 3.44 (t, $H_{l'}$), 3.27-3.21 (s, $H_{m'}$), 2.56-2.2 (broad, $H_{c'}$), 2.12-1.86 (broad, $H_{d'}$) (Figure 2b). ^{13}C NMR (125 MHz, CD_2Cl_2): δ 177.2, 173.9, 144.0, 129.36, 126.0, 72-70.1, 59.6, 50.8, 30.6, 26.0 (Figure S5b).

Measurements. ^{1}H NMR spectra were recorded at room temperature using a Bruker AM 500 (500 MHz) spectrometer with tetramethylsilane (TMS) as the external standard. ^{13}C CP-MAS NMR spectra were acquired on a Bruker 14.1 T wide-bore Avance III spectrometer equipped with a 4 mm double-resonance magic-angle-spinning (MAS) probe head. The Larmor frequency used for ^{13}C NMR is 150.92 MHz and the samples were spun at 12 kHz. Infrared spectra were recorded from a Bruker Tensor 27 Fourier-transform infrared (FTIR) spectrophotometer; 32 scans were collected at a spectral resolution of 1 cm^{-1}. The solid polymer powders were homogeneously blended with KBr before pressed to make pellets for measurement. DSC analyses were performed using a TA Q-20 differential scanning calorimeter operated at a heating rate of 10 °C/min. Relative molecular weights of the polymers were determined through gel permeation chromatography (GPC) using a Waters 510 high performance liquid chromatography (HPLC) system with DMF as the eluent and a flow rate: 0.4 mL/min. The molecular weight calibration curve was obtained from polystyrene standards. The PL emission spectra were obtained from a LabGuide X350 fluorescence spectrophotometer using a 450 W Xe lamp as the continuous light source. A small quartz cell with dimensions 0.2 × 1.0 × 4.5 cm^3 was used to accommodate the solution sample. A "right angle" geometry that fluorescence was collected at right angle to the excitation beam used in the spectral measurement. Circular dichroism (CD) spectra were recorded using a JASCO J-810 spectrometer, with sample in deionized water at a concentration of 10^{-4} M. The spectra were also

curve-fitted with the Spectra Manager program to resolve the fraction of the individual secondary structure. Dimension of the aggregate particles was determined from DLS instrument on a Malvern ZetaSizer Nano ZS90 spectrometer. A He–Ne laser operating at 633 nm was used as light source.

■ RESULTS AND DISCUSSION

Synthesis of water-soluble, ionic polymer of TP-PPLG-MEO_2

According to Scheme 1, the click reaction between the alkyne side groups of TP-PPLG and MEO_2-N_3 (1-(2-methoxyethoxy)-2-azidoethane) is the key step leading to TP-PPLG-*g*-MEO_2. Hence, the two intermediates of TP-PPLG and MEO_2-N_3, involved in the click reaction needed to be prepared primarily. TP-PPLG was synthesized from ring-opening polymerization of PLG-NCA[40,41] initiated by the amino group of TP-NH_2[38]. PLG-NCA was prepared from the facile cyclization of propargyl-glutamate (PLG)[40,41] by triphosgene whereas TP-NH_2 was prepared from a two-step synthesis procedure, including nitration of TP and the subsequent reduction of the nitro group to generate TP-NH_2. Another intermediate of MEO_2-N_3[39] was synthesized by a substitution reaction of sodium azide (NaN_3) and tosylated-MEO_2 (MEO_2-OTs), which was prepared from reaction of MEO_2 and tosyl chloride (TsCl). All intermediates (Figure S1-4. ESI*) and product were carefully purified and identified. Molecular weight and fraction of secondary structure of TP-PPLG and TP-PPLG-*g*-MEO_2 were summarized in Table 1 for comparison.

Primarily, FTIR analysis was applied to confirm the success of click reaction. Figure 1 characterized the absorption changes of the azido and acetylene functions in MEO_2-N_3 and TP-PPLG, respectively. The signals at 2130 cm^{-1}, representative of the alkyne group of TP-PPLG, and 2105 cm^{-1}, representative of the azido group of

MEO_2-N_3, are absent in the spectrum of TP-PPLG-*g*-MEO_2. Successful click reaction efficient in converting azido and acetylene groups into triazole ring should take place preferably.

We further compared ^{1}H NMR spectra of TP-PPLG and TP-PPLG-*g*-MEO_2 in Figure 2, to demonstrate the success of click reaction. In the spectrum of TP-PPLG (Figure 2a), the alkyne protons H_a resonated at 2.47 ppm as a singlet, overlapping with resonances of the alkyl protons H_c and H_d, and the solvent peaks in the range from 2.17 to 2.73 ppm. Click reaction transformed the alkyne group into triazine and therefore, the corresponding protons $H_{b'}$ of TP-PPLG-*g*-MEO_2 resonated at 5.17 ppm (Figure 2b). The resonance of CH_2 protons H_b, neighboring to alkyne group of TP-PPLG, originally located at 4.70 ppm but after click reaction, the CH_2 protons $H_{b'}$ are now neighboring to triazole ring of TP-PPLG-*g*-MEO_2 and therefore resonated at a lower filed of 5.17 ppm. Successful click reaction was therefore verified from the ^{1}H NMR spectra.

By calculating the intensity ratio of resonances H_b to H_g, number average molecular weight (M_n,17,840 g/mol, Table 1) of TP-PPLG was conveniently evaluated (Table 1) but for TP-PPLG-*g*-MEO_2, the aromatic multiplets of $H_{g'}$ cannot be detected in spectrum (Figure S4b) conducted in pure CD_2Cl_2. Aromatic multiplets can only be resolved in the spectrum (Figure 2b) conducted in d_6-DMSO containing small amounts of DCl. In this case, acidic DCl acted to rupture intramolecular hydrogen bonds (H bonds) existing in the rigid α-helical chains, converting the rigid helical chains into flexible random coils. The coil-linked TP terminals of TP-PPLG-*g*-MEO_2 chains were no longer hampered in rotation, as the original helical chains before adding DCl, therefore rendering detectable NMR signals regarding the enhanced molecular motion in the acidic solution. Therefore, molecular weight of

TP-PPLG-*g*-MEO_2 can be calculated from the intensity ratio of $H_{b'}$ to $H_{g'}$ and the result indicated a M_n of 33,000 g/mol. The calculated degrees of polymerization (DPs) of TP-PPLG and TP-PPLG-*g*-MEO_2 are in close vicinities of 105; therefore, conversion of click reaction must be quantitative to result in the close value of DPs.

The M_ns measured from GPC analysis were also included in Table 1, which are much higher than the values from ^{1}H NMR. The high value of GPC analysis is due to the early elution of the rigid polymer chains, which is especially true for the large α-helical chains. With a large diameter, the α-helical chains spend little if any time in the pores of the gels packed in the columns of GPC; therefore, they elute quickly to result in M_n much higher than the polymer standard (polystyrene) of the same M_n. The early elution also resulted in M_ns much higher than the more realistic M_ns determined from ^{1}H NMR.

Secondary structure of TP-PPLG and TP-PPLG-*g*-MEO_2

FTIR analysis provided information regarding the secondary structures of TP-PPLG and TP-PPLG-*g*-MEO_2. Analysis of these spectra using the second-derivative technique[42] revealed that the amide I band at 1655 cm^{-1} is characteristic of the α-helical chain. For polypeptides possessing a β-sheet conformation, the amide I band appeared at 1627 cm^{-1} while for random coil or turn populations, a characteristic peak at 1693 cm^{-1} was resolved. Besides, the free C=O of the peptide side chains provided a signal at 1740 cm^{-1}. Based on the characteristic peaks, the absorptions in the range from 1500 to 1800 cm^{-1} were de-convoluted into a series of Gaussian curves (Figure 3), to evaluate fraction of each of the peaks. Table 1 gave the fitting results of the amide I group for α-helix, β-sheet and random coil structures. Clearly, peptide chains of TP-PPLG-*g*-MEO_2 are higher in the content of

α-helical conformation compared to TP-PPLG, which demonstrated the role of long MEO_2 chains in promoting α-helical chain. The α-helical chain can be regarded as rigid rod stabilized through intramolecular H bond interactions whereas the β-sheet is structure stabilized by intermolecular H bond interactions[43]. Comparatively, random coil is flexible chain least in stability considering its fewer and irregular H bond interactions compared to α-helical and β-sheet structures. The long MEO_2 side groups sterically shielded the main chain amides from intermolecular H bonding to other peptide chains and thus favored the formation of α-helix with predominant intramolecular H bonds. Based on the stability reason, certain fractions of the least stable coil chains of TP-PPLG also became parts of the stable α-helical chains in TP-PPLG-g-MEO_2.

AIE character of TP-PPLG-*g*-MEO_2

The AIE character of TP-PPLG-*g*-MEO_2 was primarily evaluated from the solution emission responses toward concentration and aggregation. Effect of concentration was demonstrated by the solution emission spectra of TP-PPLG-*g*-MEO_2 in dichloromethane (Figure 4a). In contrast to the emission quenching caused by solution thickening, emission of TP-PPLG-*g*-MEO_2 nevertheless became greater in intensity as the solution concentration of TP-PPLG-*g*-MEO_2 was increased from 2.5 x 10^{-7} M to 2.5 x 10^{-5} M (relative to number of polymer chains). Here, solution emission spectra in Figure 4a consisted of two overlapped bands, representative of the short-wavelength monomer emission at 420 nm and the long-wavelength aggregate emission at 480 nm, respectively. Fraction of aggregate emission was actually raised by concentration. High concentration raised the aggregation level of TP terminals, which directly enhanced the aggregate emission.

Aggregation of TP terminals in solvent/nonsolvent mixtures was also used in this study to identify the AIE effect. With this respect, diethyl ether (Et_2O) was employed as nonsolvent to induce solution aggregation of TP terminals in good solvent of dimethylforamide (DMF). Upon irradiation at 340 nm, dilute solution (3×10^{-6} M) of TP-PPLG-*g*-MEO_2 in DMF already emitted with discernible intensity (Figure 4b) and adding Et_2O (while keeping concentration of TP-PPLG-*g*-MEO_2 at 3×10^{-6} M) resulted in progressive intensity gains on both monomer and aggregate emissions. Upon adding Et_2O, TP terminals tend to be more associated together and therefore be more hampered in rotational motion, thereby promoting the AIE-related emission.

Secondary structure in relation to the AIE-related emission

As illustrated in Scheme 2, peptide chains of TP-PPLG-*g*-MEO_2 are subjected to conformational changes, from the initial α-helix to β-sheet or to random coil, by different experimental conditions applied and the conformational changes in correlating the AIE activity are primarily discussed here before entering detailed results. In general, mutual approaches (aggregation) of the TP terminals, as the key controlling molecular rotation and AIE-related emission, are affected by the dimension and rigidity of the peptide chains connecting to TP units. In speaking of chain dimension, rigid α-helical rods, who's reported diameters (15 – 26 Å[33, 44,45]) are larger than the molecular width (9 Å) of TP unit, are effective in blocking the intermolecular approaches of the TP terminals 3-dimensionally. Hampered aggregation of TP terminals in the α-helical chains is detrimental for AIE activity, and therefore weakens the luminescence of the α-helical peptide chains. Compared to TP terminals in the helical chains, β-sheet-linked TP terminals are easier in associating together to form aggregates since the 2D β-sheet chains are not so

spatially repulsive to each other as the bulky, 3D helical chains. Higher emission is expected for the TP terminals in the β-sheet than in the α-helical chains. Among all three secondary structures, flexible random coil is no double the one best at moving TP terminals to nearby vicinities regarding the free segmental motion of the flexible coil chains; thereby, we expected a high aggregate emission for the TP-PPLG-*g*-MEO_2 chains in random coil conformation.

Most of the TP-PPLG-*g*-MEO_2 chains in the aqueous solution are in the α-helical conformation and because that they can be conveniently converted into β-sheet and random coil chains in the NaCl salt and the alkaline solutions, respectively, the induced helix-to-sheet and helix-to-coil transitions and the corresponding emission variations will be identified and discussed separately below.

Conformational transformation and emission variation in the salt solution

For amphiphilic polymers in the aqueous solutions, adding salts[46-49] were reported to affect the solubility of the polymers toward water and the corresponding lower critical solution temperature (LCST) of the salt solutions. Taking the aqueous solution of poly(*N*-isopropyl acrylamide) (PNIPAM)[49] as an example, cations of the salts preferably reacted with the side-chain amide groups of PNIPAM, resulting in dehydration of amide side groups and the depression of LCST upon increasing salt content in the aqueous solution. For TP-PPLG-g-MEO_2, we also observed the decrease of LCST ("salting-out" effect) upon increasing NaCl content in the aqueous solution (Figure S9). As has been pointed out before, the "salting-out" effect is therefore not the focus of this study; instead, the salt-induced conformational transformation and emission change are more attractive to us.

Figure 5 showed the emission enhancement caused by adding NaCl to the aqueous solution of TP-PPLG-MEO_2. With increasing salt content in the solution, both monomer and aggregate emissions gradually gained their intensities. The intensity ratio between aggregate and monomer emissions (I_a/I_m) was then calculated and summarized in Table 2, which indicated that that I_a/I_m increased from 0.677 to 0.825 as the salt content was increased from 0 M to 0.154 M. A higher value of I_a/I_m that correlates with greater aggregation level of the TP terminals was therefore involved in the newly-developed secondary structure induced by NaCl. The enhanced aggregation is supposed to be responsible for the observed enhanced emission of the aqueous salt solution.

We then recorded circular dichroism (CD) spectra (Figure 6) to characterize the corresponding conformation responsible for the enhanced emission of the salt solutions. The α-helical structure was characterized by a triply inflected spectrum[39], corresponding to two negative bands at 208 and 222 nm and a strong positive band at 192 nm. The β-sheet structure was characterized by a negative minimum band near 218 nm and a positive maximum near 198 nm. The random coil structure was characterized by a small positive band at 218 nm and a negative band near 200 nm. Figure 6 showed that the gradual transformation of α-helical conformation, in correlating the slight change of the ellipticity ratio ($[\theta]_{222}/[\theta]_{208}$), upon increasing NaCl content from 0 to 0.154 M. Disregarding the slight change of the ellipticity ratio, significant spectral variation occurred in the short-wavelength region in which the main band shifted from 192 nm, characteristic of α-helical chains, to 198 nm, typical of β-sheet chains. The spectra were then fitted, by using Spectra Manager program, to resolve percentages of each secondary structure and the results illustrated in the inset of Figure 6 indicated that content of α-helical chain was decreased from 72.9 % to

23.3 %, in corresponding to the increase of β-sheet chain from 3 % to 54.1 % (also, refers to the calculated results in Table S1). Therefore, high fraction of 3D α-helical chains had been transformed into 2D β-sheet chains by NaCl salts added in the solution. The intimately-packed β-sheet chains (Scheme 2) are therefore responsible for the better emission of the salt solution but what is the driving force causing this interesting helix-to-sheet transition? The ^{1}H NMR analysis on the salt solutions may give us clue to evaluate the potential cause leading to the helix-to-sheet transition.

It was envisaged that NaCl additives complexed to both the amide groups of the main chain and the heteroatoms (nitrogen and oxygen) of the side chain, pulling both chain segments closer enough to form intimately-packed β-sheet chains. Such structural transformation was indirectly demonstrated by the ^{1}H NMR band shape analysis on the solutions of TP-PPLG-MEO_2 in D_2O containing different amounts of NaCl (Figure 7). The band shape analysis was previously utilized in the study of rotation-induced conformational changes.[51] Main principle behind this analysis is that fast conformational exchanges caused by the fast molecular rotations would result in sharp resonance peaks, whereas the slower exchanges due to restricted molecular rotation broaden the resonance peaks. Moreover, in many polymer systems[52,53], the rotational restriction imposed by the polymer chains is so effective that the corresponding resonance peaks become weakening or disappear. In the present study, the concentration of TP-PPLG-*g*-MEO_2 was kept at a constant value of 1.5 x 10^{-5} M but the resonance peaks due to protons in the main (H_b) and side ($H_{c\text{-}k}$) groups still became broadened and weakened with increasing NaCl from 0 to 0.154 M. Presumably, the sodium cations complexed to the amide C=O groups of the main chains and the heteroatoms (nitrogen and oxygen) of the MEO_2 side chains and hampered the rotations of the main and side chain groups to result in the broadening

and weakening of the resonance peaks, due to the clumsy response of the corresponding chemical bonds towards the stimuli of external magnetic field.

In the salt solution, intramolecular H bonds, originally prevalent in α-helical chains, were ruptured and replaced by intermolecular ionic bonds, between the sodium cations and the amide main chain groups, present in the β-sheet structure. Complexation of sodium cations and MEO_2 side groups also functioned to hold the neighbouring MEO_2 side groups to closer distances beneficial for the intimately-packed β-sheet structure. When linked by the intimately-packed β-sheet chains, TP terminals are easier to associate together, resulting in emission with higher efficiency than the helix-linked TP terminals, whose mutual approaches were seriously blocked by the large helical rods.

Conformational transformation and emission variation in the alkaline solution

Poly(L-glutamic acid) was reported to undergo a helix-to-coil transition at pH value of 6.18.[53,54] A similar transition was observed in β-cyclodextrin (β-CD)-grafted PPLG[55], however, at a higher pH range in between 11 and 11.5 due to the steric hindrance or the stable helical structure inherited by the β-CD grafts. Likewise, the helix-to-coil transition was observed for TP-PPLG-*g*-MEO_2 system in alkaline solution, which helps evaluate effect of chain conformation on AIE activity. As illustrated in Figure 8, emission of the aqueous TP-PPLG-*g*-MEO_2 solution indeed depends on the applied pH of the solution. At pH $\leq$ 7, the aqueous solutions emitted similarly without notable variation. However, when NaOH was gradually added to the solution, the initial monomer emission was continuously transformed into a major aggregate emission with intensity much higher than the initial monomer emission. The aggregate emission at 520 nm gradually developed its intensity in alkaline

solutions and at pH 13.6, the aqueous solution emitted with a large aggregate emission, whose intensity is at least 8-fold to that at pH 7. Easy intermolecular aggregation of the TP terminals chains must be prevalent in the alkaline solution, in order to emit with a major aggregate emission shown in Figure 8.

The conformational transformation was also traced by CD spectra (Figure 9). By increasing pH from 2 to 11, there are only slight variation on the ellipicity ratio of $[\theta]_{222}/[\theta]_{208}$. Major conformational transformation occurred only at pH > 12 according to the spectral change that the triply inflected peaks reduced to a small doubly inflected dichroic spectrum. At this stage, the majority of α-helical chains should have been converted into random coils by NaOH.

Conformational transformation of the peptide chains affected the extent of aggregation and the AIE-related emission of the peptide-linked TP terminals. As illustrated in Scheme 2, with mobile segmental motion, the flexible peptide chains easily moved their TP terminals to closer range to become highly-aggregated TP phase, which emitted with strong aggregate emission with intensity much higher than the TP units linked by the less-mobile α-helical or β-sheet structure.

Luminescent responses of α-helical, β-sheet and random coil chains toward bovine serum albumin.

As large globular protein (66 kDa) consisting of 583 amino acid residues in a single polypeptide chain, bovine serum albumin (BSA)[56] is one of the most intensively-studied proteins in the biochemistry or biomedical science due to its structural similarity with human serum albumin (HSA)[57]. In practice, BSA was often used as a complexing material for certain dyes and probes, in which the emission

response[58] can be used to study the binding mechanisms. Since we can prepare luminescent polypeptides of three secondary structure, it will be interesting for use to evaluate the possibility of the individual secondary peptide chains as luminescent probes for BSA; particularly, the luminescence responses of TP-PPLG-*g*-MEO_2 toward complexing with BSA are reflections of the aggregation level of the TP terminals linked by peptide chains of different secondary structures.

Experimentally, α-helix, random coil and β-sheet chains prepared from the respective neutral, alkaline and salt solutions were used for complexing with different amounts of BSA. The results suggested that solution emissions of random coil (Figure 10a) and β-sheet chains (Figure 10b) are both decreased by the inclusion of BSA, which is distinctly different from the intensity gain observed in the emission spectra (Figure 11) from the α-helical chain. Consider the AIE-related emission is closely related to the aggregation level of the luminogenic TP, the emission reductions observed in the alkaline and salt solutions should be correlated with the dissociation of the aggregated TP terminals. Particularly, regarding the large reduction of the aggregate emission (Figure 10a) in the alkaline solution, dissociation of the TP aggregates in the random coil chains must be significant in order to correlate with the large spectral change. Comparatively, that the emission loss (Figure 10b) is minor for the salt solution indicated that there are only slight dissociation of TP terminals during the complexation of the β-sheet chains with BSA. The emission gain (Figure 11) observed for the α-helical chains is therefore correlated with the enhanced rotational restriction of the TP terminals.

The large emission reduction observed in the alkaline solutions suggested the preferable complexation of the random coil chains to BSA; most likely, the flexible coil chains readily diffused into the interior domain of the large BSA chains, to result

in exclusive reaction responsible for the large reduction on the aggregate emission observed in Figure 10a. With low structural stability, flexible coil chains were subjected to significant conformational change when complexed with BSA. It was then envisaged that stable chains with structural integrity are less prone to undergo conformational change during complexation with BSA. When complexed to BSA, the α-helical chains, with structural integrity maintained by intramolecular H bonds, and the β-sheet conformation, stabilized by intermolecular H bonds, are therefore suggested to undergo minor structural changes and less emission variations compared to the unstable random coil. When entered into the domain of BSA, the stable α-helical rod remained in the rigid conformation and rotational restriction of the TP terminals were further reinforced by the viscous matrix of BSA, thereby resulting in the enhanced emission observed in Figure 11. According to the small emission variation shown in Figure 10b, the less stable β-sheet chain may undergo slight conformational change when complexed with BSA. Some intermolecular H bonds in the β-sheet chains may be ruptured to result in the dissociation of TP aggregates and the slight emission reduction.

■ CONCLUSION

Amphiphilic polypeptide of TP-PPLG-*g*-MEO_2 with an AIE-active TP terminal and ether MEO_2 side groups was prepared from ring opening polymerization of PLG-NCA monomer and the following click reaction. TP-PPLG-*g*-MEO_2 was characterized to be active in AIE properties according to its emission behavior toward concentration and aggregation.

In aqueous solution, the majority of α-helical chains of TP-PPLG-*g*-MEO_2 can be converted into β-sheet and random coil structures by NaCl salt and NaOH base,

respectively. With better aggregation tendency, TP terminals linked by the 2D β-sheet chains emitted with higher emission intensity than TP terminals linked by the large 3D helical rods. TP terminals linked by flexible random coils are the most mobile ones, rendering highly-aggregated TP terminals with emission intensity higher than TP terminals linked by less-mobile helix and β-sheet chains. Role of secondary structure of peptide chain in determining the aggregation tendency and the AIE-related emission behavior was therefore evaluated.

Complexation of BSA resulted in emission enhancement of the helix-linked TP terminals due to the reinforced rotational restriction imposed by BSA. In contrast, large emission reduction was observed in the TP terminals linked by the random coil chains and most likely, significant dissociation of the aggregated TP terminals occurred during complexation of the coil chains with BSA. Comparatively, **s**tructural change in the β-sheet chains is small regarding the slight reduction on the emission intensity upon complexing with BSA**.**

■ ASSOCIATED CONTENT

Supporting Information

Table S1 and Figures S1 – S9. This material is available free of charge via the Internet at http://pubs.acs.org.

■ AUTHOR INFORMATION

Corresponding Author

* E-mail jlhong@mail.nsysu.edu.tw; Tel +886-7-5252000 ext 4065 (J.-L.H.).

Notes

The authors declare no competing financial interest.

■ ACKNOWLEDGEMENTS

We appreciate the financial support from the Ministry of Science and Technology, Taiwan, under the contract no. NSC 102-2221-E-110-084-MY3 and 104-2221-E-110 -050.

■ REFERENCES

1 J. Luo, Z. Xie, J. W. Y. Lam, L. Cheng, H. Chen, C. Qiu, H. S. Kwok, X. Zhan, Y. Liu, D. Zhu and B. Z. Tang, *Chem. Commun.,* 2001, 1740.

2 B. Z. Tang, X. Zhan, G. Yu, P. P. S. Lee, Y. Liu and D. Zhu, *J. Mater. Chem.,* 2001, **11**, 2974.

3 Y. Hong, J. W. Y. Lam and B. Z. Tang, *Chem. Commun.,* 2009, 4332.

4 D. Ding, K. Li, B. Liu and B. Z. Tang, *Acc. Chem. Res.,* 2013, **46**, 2441.

5 Z. Zhao, J. W. Y. Lam and B. Z. Tang, *J. Mater. Chem.,* 2012, **22**, 23726.

6 M. Wang, G. Zhang, D. Zhang, D. Zhu and B. Z. Tang, *J. Mater. Chem.,* 2010, **20**, 1858.

7 Z. Zhao, J. W. Y. Lam and B. Z. Tang, *Soft Matter.* 2013, ***9***, 4564.

8 *Aggregation-Induced Emission: Fundamentals*, A. Qin, and B. Z. Tang, ed., John Wiley & Sons, Ltd, NY, 2013.

9 J. Mei, Y. Hong, J. W. Y. Lam, A. Qin, Y. Tang, and B. Z. Tang, *Adv. Mater.,* 2014, **26**, 5429.

10 H. Wang, E. Zhao, J. W. Y. Lam and B. Z. Tang, *Maters Today,* 2015, April.

11 Z. Li, Y. Dong, B. Mi, Y. Tang, M. Häussler, H. Tong, Y. Dong, J. W. Y. Lam, Y. Ren, H. H. Y. Sung, K. S. Wong, P. Gao, L. D. Williams, H. S. Kwok and B. Z. Tang, *J. Phys. Chem. B* 2005, **109**, 10061.

12 J. Chen, C. C. W. Law, J. W.Y. Lam, Y. Dong, S. M. F. Lo, I. D. Williams, D. Zhu and B. Z. Tang, *Chem. Mater.,* 2003, **15**, 1535.

13 Z. Zhao, C. Y. K. Chan, S. Chen, C. Deng, J. W. Y. Lam, C. K. W. Jim, Y. Hong, P. Lu, Z. Chang, X. Chen, P. Lu, H. S. Kwok, H. Qiu, H. and B. Z. Tang, *J. Mater. Chem.,* 2012, **22**, 4527.

14 J. Huang, X. Yang, J. Wang, C. Zhong, L. Wang, J. Qin, Z. Li, *J. Mater. Chem.,* 2012, **22**, 2478.

15 J. Huang, N. Sun, J. Yang, R. Tang, Q. Li, D. Ma, J. Qin and Z. Li, *J. Mater. Chem.,* 2012, **22**, 12001.

16 J. Huang, N. Sun, Y. Dong, R. Tang, P. Lu, P. Cai, Q. Li, D. Ma , D. Qin and Z. Li, *Adv. Funct. Mater.,* 2013, **23**, 2329.

17 X. Chen, X. Y. Shen, E. Guan, Y. Liu, A. Qin, J. Z. Sun and B. Z. Tang, *Chem. Commun.,* 2013, **49**, 1503.

18 X. Wang, J. Hu, T. Liu, G. Zhang and S. Liu, *J. Mater. Chem.,* 2012, **22**, 8622.

19 X. Huang, X. Gu, G. Zhang and D. Zhang, *Chem. Commun.,* 2012, **48**, 12195.

20 C. Li, T. Wu, C. Hong, G. Zhang and S. Liu, *Angew. Chem. Int. Ed.,* 2012, **51**, 455.

21 Y. Yu, A. Qin, C. Feng, P. Lu, K. M. Ng, K. Q. Luo and B. Z. Tang, *Analyst,* 2012, **137**, 5592.

22 K. Tohyama and W. C. Miller, *Nature,* 1981, **289**, 813.

23 Y. Bae, S. Fukushima, A. Harada and K. Kataoka, *Angew. Chem., Int. Ed.,* 2003, **42**, 4640.

24 H. Tang and D. Zhang, *J. Polym. Sci., Part A: Polym. Chem.,* 2010, **48**, 2340.

25 A. Gitsas, G. Floudas, M. Mondeshki, H. W. Spiess, T. Aliferis, H. Iatrou and N. Hadjichristidis, *Macromolecules,* 2008, **41**, 8072.

26 H. Tang, L. Yin, H. Lu and J. Cheng, *Biomacromolecules,* 2012, **13**, 2609.

27 Y. Cheng, C. He, C. Xiao, J. Ding, H. Cui, X. Zhuang and X. Chen, *Biomacromolecules,* 2013, **14**, 468.

28) V. K. Kotharangannagari, A. Sanchez-Ferrer, J. Ruokolainen and R. Mezzenga, *Macromolecules,* 2011, **44**, 4569.

29 J. Huang and A. Heise, *Chem. Soc. Rev.,* 2013, **42**, 7373.

30 Y. Shen, X. Fu, W. Fu and Z. Li, *Chem. Soc. Rev.,* 2015, **44**, 611.

31 H. Tian, Z. Tang, X. Zhuang, X. Chen and X. Jing, *Prog. in Polym. Sci.,* 2012, **37**, 237.

32 S. Zhang and Z. Li, *J. Polym. Sci., Part B, Polym. Phys.,* 2013, **51**, 546.

33 P, Doty, J. H. Bradbury and A. M. Holtzer, *J. Am. Chem. Soc.,* 1956, **78**, 947.

34 V. Pokorná, D. Výprachtický and J. Pecka, *Macromol. Biosci.,* 2001, **1**, 185.

35 K. T. Kim, C. Park, G. W. M. Vandermeulen, D. A. Rider, C. Kim, M. A. Winnik and I. Manners, *Angew. Chem.,* 2005, **117**, 8178.

36 S. T. Li, Y. C. Lin, S. W. Kuo, W. T. Chuang and J. L. Hong, *Polym. Chem.,* 2012, **3**, 2393.

37 K. Y. Shih, T. S. Hsiao, S. L. Deng and J. L. Hong, *Macromolecules,* 2014, **47**, 4037.

38 S. T. Li, Y. C. Lin, S. W. Kuo, W. T. Chuang, and J. L. Hong, *Polym. Chem.,* 2012, **3**, 2393.

39 Y. Cheng, C. He, C. Xiao, J. Ding, X. Zhuang and X. Chen, *Polym. Chem.,* 2011, **2**, 2627.

40 Y. C. Lin and S. W. Kuo, *Polym. Chem.,* 2012, **3**, 162.

41 Y. C. Lin and S. W. Kuo, *Polym. Chem.,* 2012, **3**, 882.

42 Y. Zhang, H. Lu, Y. Lin and J. Cheng, *Macromolecules,* 2011, **44**, 6641.

43 P. Papadopoulous, G. Floudas, H. A. Klok, I. Schnell and T. Pakula, *Biomacromolecules,* 2004, **5**, 81.

44 T. Torii, T. Yamashita, H. Ushiki and K. Horie, *Eur. Polym. J.,* 1993, **29**, 465.

45 F. A. Bovey and G. V. D. Tiers, *Adv. Polym. Sci.,* 1963, **3**, 139.

46 J. P. Magnusson, A. Khan, G. Pasparakis, A. Q. Saeed, W. X. Wang and C. Alexander, *J. Am. Chem. Soc.,* 2008, **130**, 10852.

47 R. Freitag and F. Garret-Flaudy, *Langmuir,* 2002, **18**, 3434.

48 Y. Cheng, C. He, C. Xiao, J. Ding, X. Zhuang and X. Chen, *Polym. Chem.,* 2011, **2**, 2627.

49 J. F. Lutz, O¨. Akdemir And A, Hoth, *J. Amer. Chem. Soc.,* 2006, **128**, 13046.

50 J. Hwang and T. Deming, J. *Biomacromolecules,* 2001, **2**, 17.

51 J. Chen, C. C. W. Law, J. W. Y. Lam, Y. Dong, S. M. Lo, I. D. Williams, D. Zhu and B. Z. Tang, *Chem. Mater.,* 2003, **15**, 1535.

52 C. T. Lai, R. H. Chien, S. W. Kuo and J. L. Hong, *Macromolecules,* 2011, **44**, 6546.

53 C. M. Yang, Y. W. Lai, S. W. Kuo and J. L. Hong, *Langmuir,* 2012, **28**, 15725.

54 R. Zimmermann, T. Kratzmu, D. Erickson, D. Li, H. G. Braun and C. Werner, *Langmuir,* 2004, **20**, 2369.

55 Y. C. Lin, P. I. Wang and S. W. Kuo, *Soft Matter,* 2012, **8**, 9676.

56 Y. Moriyama, D. Ohta, K. Hadiya, Y. Mitsui and K. J. Takeda, *Protein Chem.,* 1996, **15**, 265.

57 X. M. He and D. C. Carter, *Nature,* 1992, **358**, 209.

58 Y. Z. Zhang, B. Zhou, X. P. Zhang, P. Huang, C. H. Li and Y. Liu, *J. Hazard. Mater.,* 2009, **163**, 1345.

Table 1 Molecular Weights and fraction of secondary structures of TP-PPLG and TP-PPLG-*g*-MEO_2

Sample	Molecular weight				Secondary structure		
	M_n[a]	PDI[a]	M_n[b]	DP[b]	A_{helix}[c]	A_{sheet}[c]	A_{rod}[c]
TP-PPLG	53,000	1.15	17,838	104.5	72.7	15.2	12.1
TP-PPLG-g-MEO_2	156,000	1.22	32,999	105.2	89.4	4.9	5.7

[a] Obtained from GPC. [b] Determined from ^{1}H NMR (calculate from peak ratio between resonances H_b and H_g in TP-PPLG and between $H_{b'}$ and $H_{g'}$ in TP-PPLG-*g*-MEO_2). [c] Determined from deconvoluting the infrared absorption peaks in Figure 4.

Table 2 The intensity maxima of monomer (I_m) and aggregate (I_a) emissions in Figure 6 and the calculated ratio of I_a/I_m.

NaCl concentration	I_m[a]	I_a[b]	I_a/I_m
0 M	415	281	0.677
0.017 M	489	312	0.638
0.051 M	522	335	0.641
0.085 M	568	391	0.688
0.119 M	591	466	0.788
0.154 M	606	500	0.825

[a] Intensity of monomer emission at 420 nm [b] Intensity of aggregate emission at 480 nm.

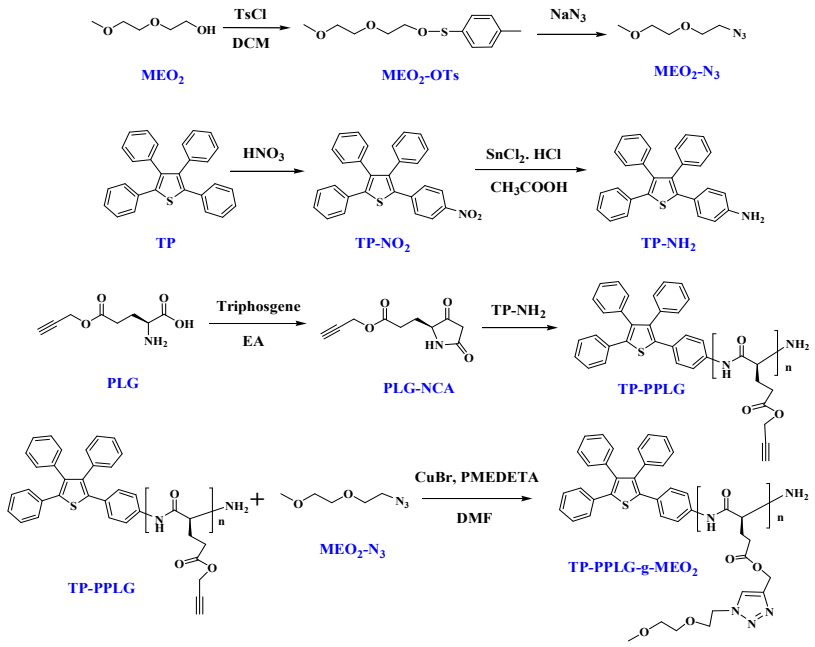

Scheme 1. Syntheses of MEO_2-N_3,TP-NH_2, and PLG-NCA monomer for the ring-opening polymerization by TP-NH_2 and the following click reaction to obtain TP-PPLG-*g*-MEO_2.

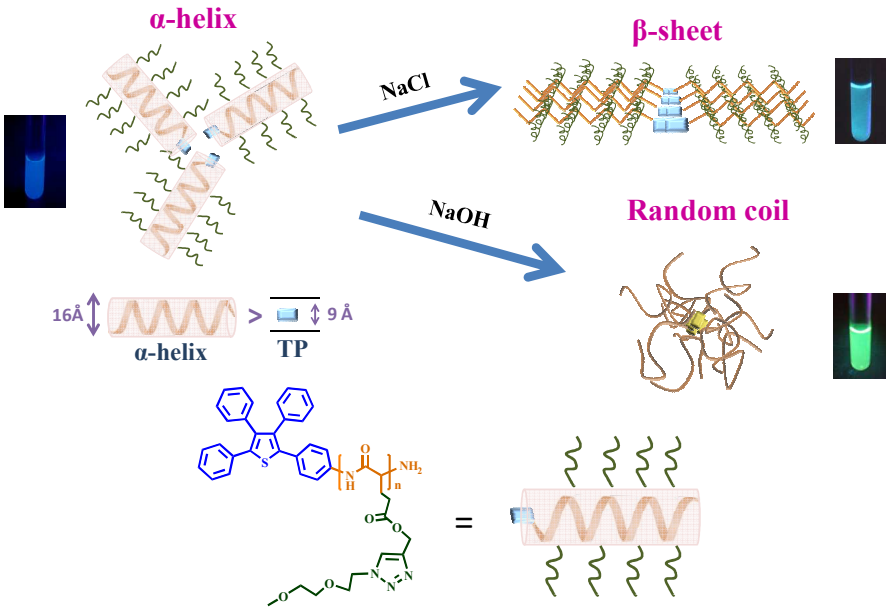

Scheme 2. Conformational changes of TP-PPLG-*g*-MEO_2 from α-helix to β-sheet in the aqueous salt solution and from α-helix to random coil in the alkaline aqueous solution, respectively.

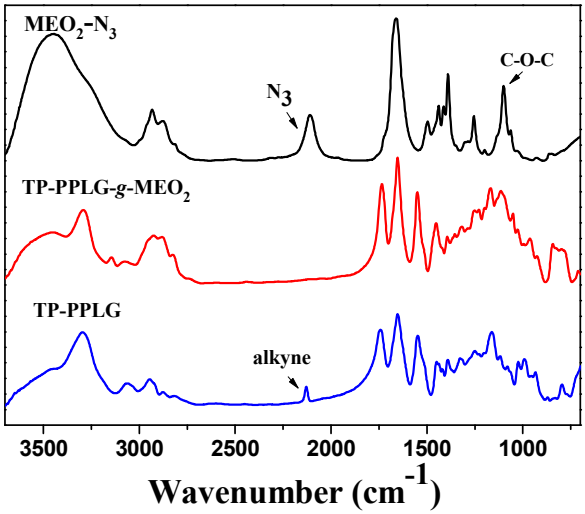

Figure 1. Solid FTIR spectra of MEO_2-N_3, TP-PPLG and TP-PPLG-*g*-MEO_2.

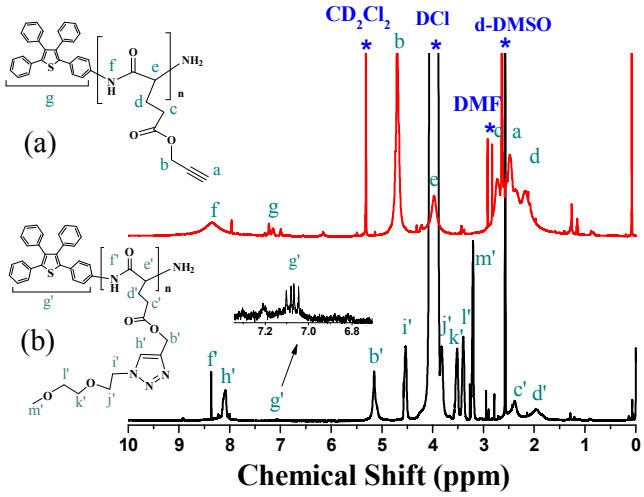

Figure 2. ^{1}H NMR spectra of (a) TP-PPLG (in d_6-DMSO) and (b) TP-PPLG-*g*-MEO_2 (in d_6-DMSO + DCl (tiny)).

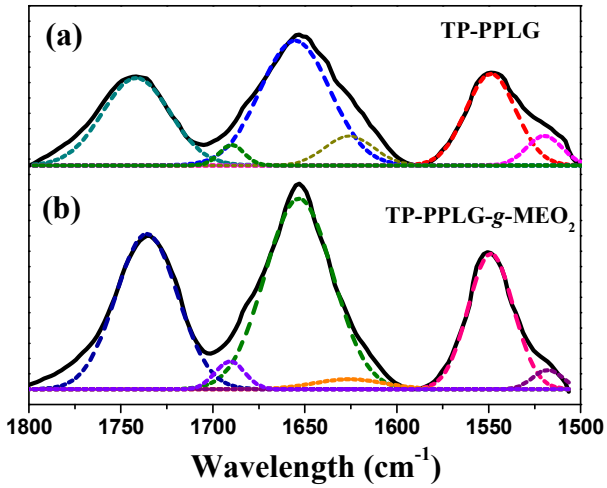

Figure 3. Curve-fitting of the FTIR spectra of (a) TP-PPLG and (b) TP-PPLG-*g*-MEO_2 in the spectral range from 1500 to 1800 cm^{-1}.

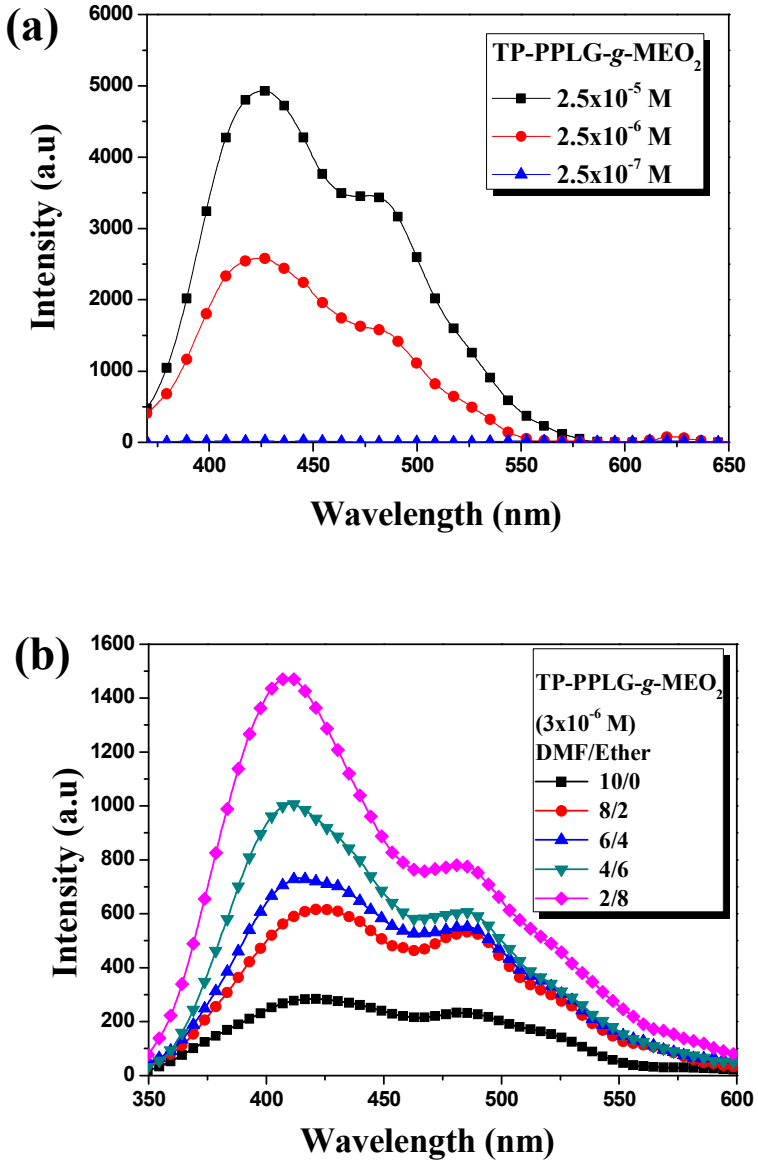

Figure 4. Solution emission spectra of (a) TP-PPLG-*g*-MEO_2 in dichloromethane of different concentration and in (b) solution mixtures of dimethyl foramide (DMF)/diethyl ether (λ_{ex} = 340 nm).

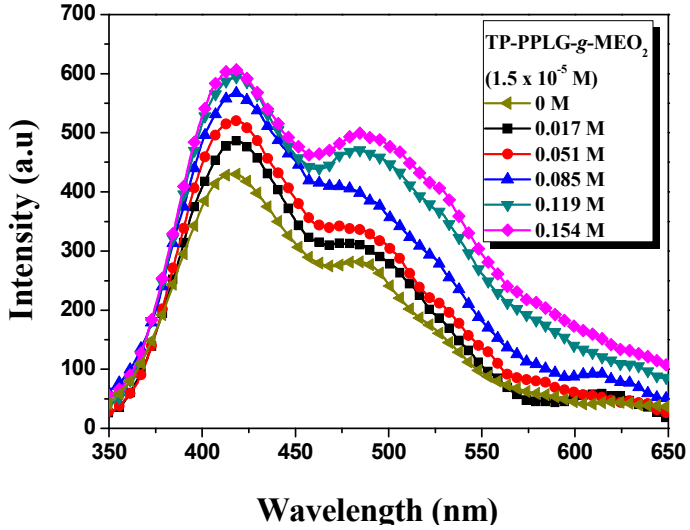

Figure 5. Emission spectra of the aqueous solution of TP-PPLG-*g*-MEO_2 ($1.5x10^{-5}$ M) containing different amounts of NaCl (λ_{ex} = 340 nm).

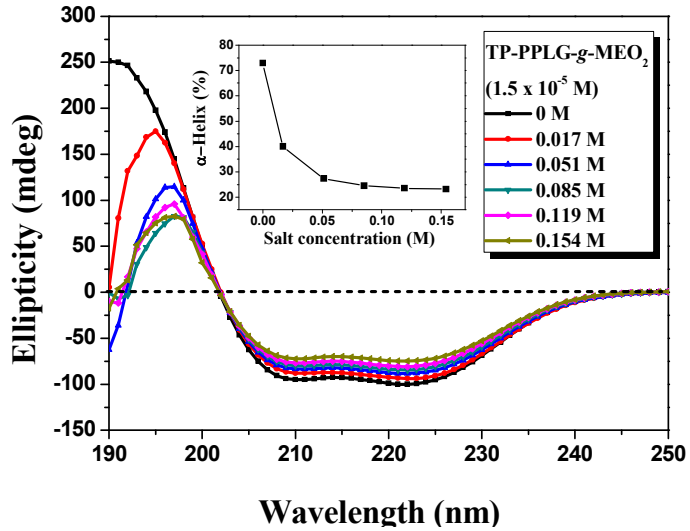

Figure 6. Circular dichroism spectrum of the aqueous solution of TP-PPLG-*g*-MEO_2 (= $1.5x10^{-5}$ M) containing different amounts of NaCl and the calculated fraction of α-helix vs. the amounts of NaCl (inset) in the solution..

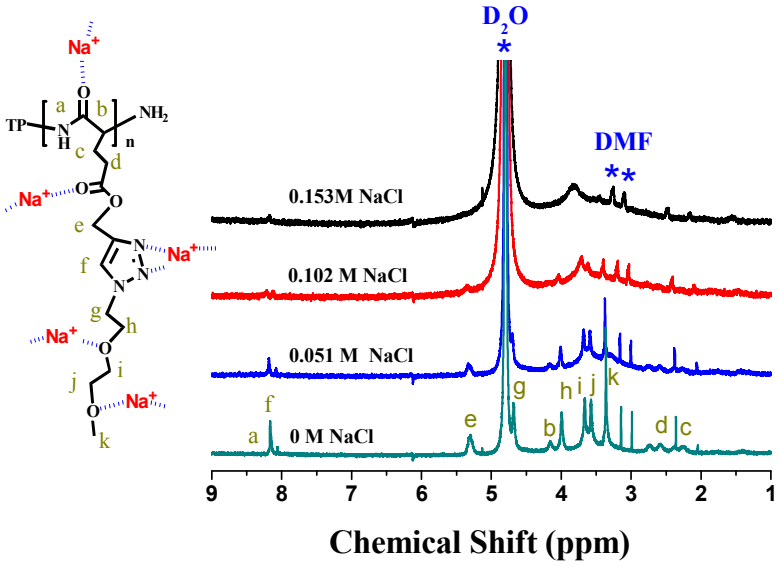

Figure 7. ^{1}H NMR spectra of TP-PPLG-*g*-MEO$_2$ (= 1.5x10^{-5} M) in D$_2$O containing different amounts of NaCl.

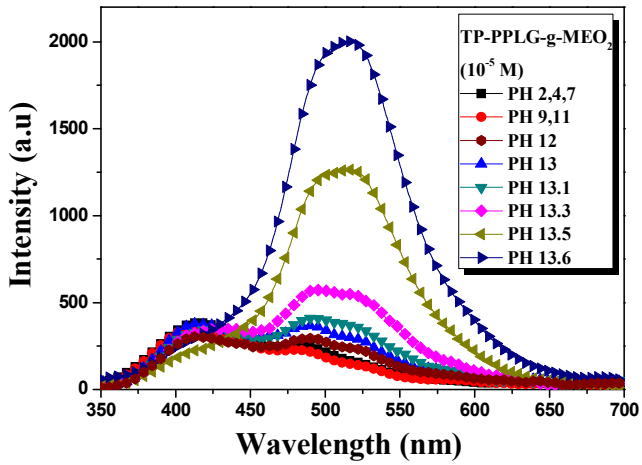

Figure 8. Emission spectra of the aqueous TP-PPLG-*g*-MEO$_2$ (= 10^{-5} M) solutions at different pHs (λ_{ex} = 340 nm).

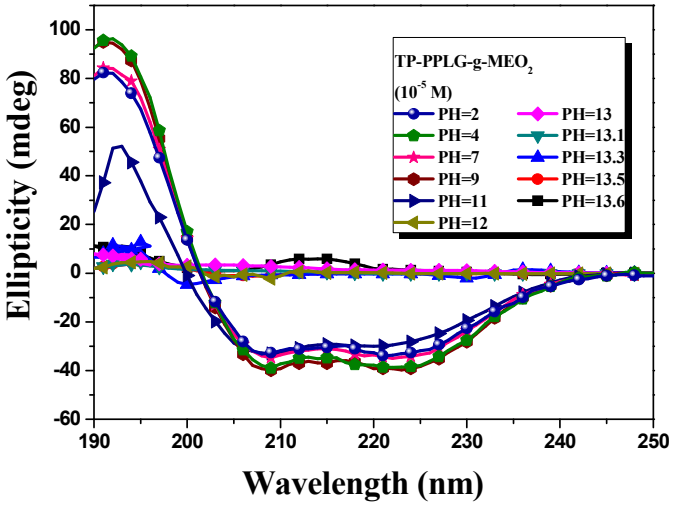

Figure 9. Circular dichroism spectrum of the aqueous TP-PPLG-*g*-MEO_2 (= 10^{-5} M) solutions at different pHs.

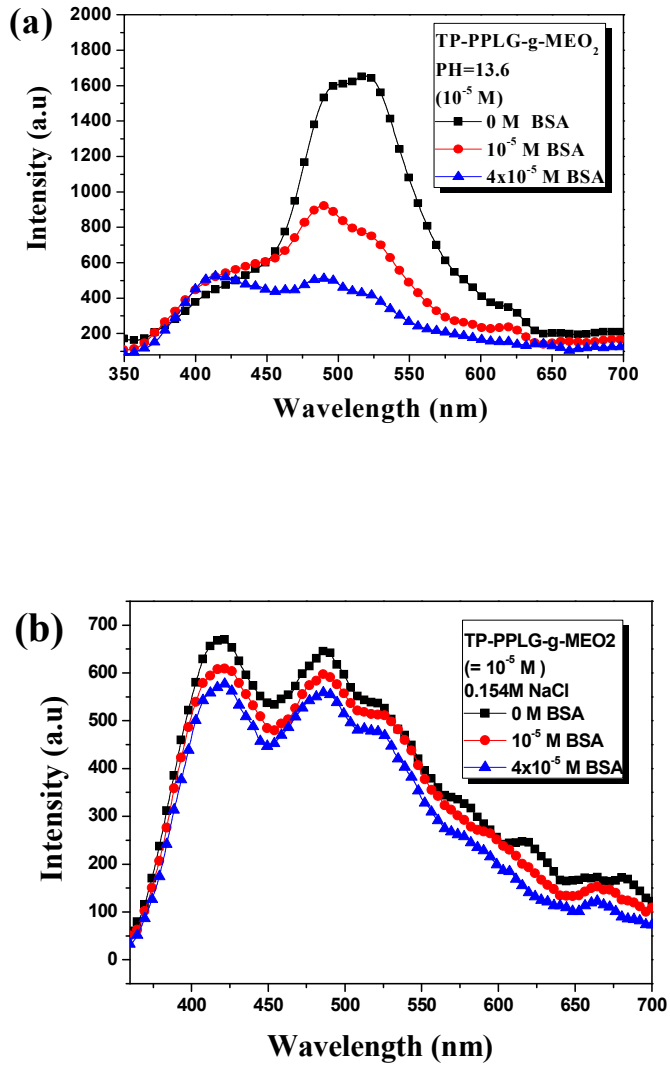

Figure 10. Emission spectral variations of the aqueous TP-PPLG-*g*-MEO_2 (10^{-5} M) solution in (a) alkaline solution (pH = 13.6) and in (b) neutral solution containing NaCl (0.156 M) towards different amounts of BSA from 0 to 4 x 10^{-5} M (λ_{ex} = 340 nm).

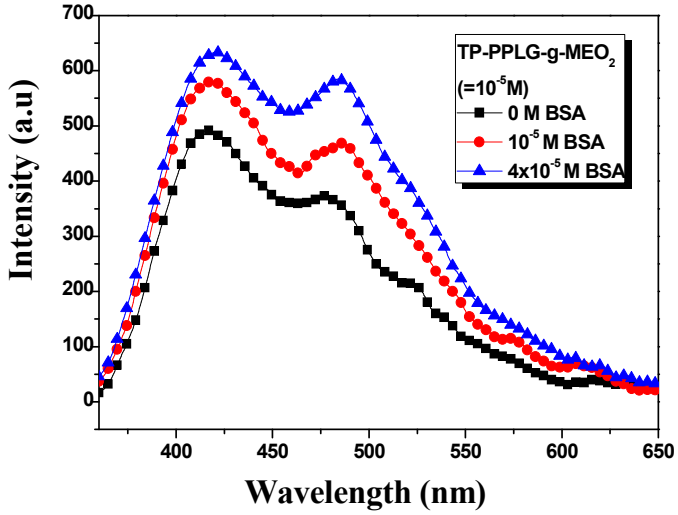

Figure 11. Emission spectra variation of the aqueous TP-PPLG-*g*-MEO_2 (10^{-5}M) solutions towards different amounts of BSA from 0 to 4 x 10^{-5} M (λ_{ex} = 340 nm).

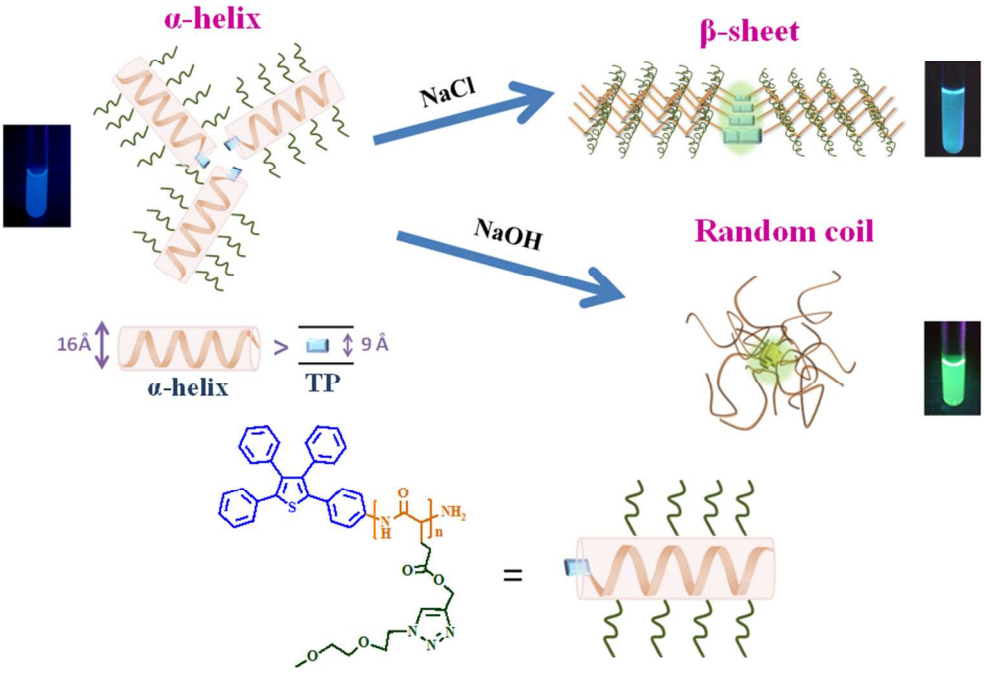

254x190mm (96 x 96 DPI)